Aerospace Science and Technology 49 (2016) 80–87

Contents lists available at ScienceDirect

Aerospace Science and Technology

www.elsevier.com/locate/aescte

Assessment of conservative force models from GRACE accelerometers and precise orbit determination

Andrés Calabia [a,b], Shuanggen Jin [a,c,*]

[a] Key Laboratory of Planetary Science, Shanghai Astronomical Observatory, Chinese Academy of Sciences, Shanghai 200030, China
[b] University of Chinese Academy of Sciences, Beijing 100049, China
[c] Department of Geomatics Engineering, Bulent Ecevit University, Zonguldak 67100, Turkey

ARTICLE INFO

Article history:
Received 4 June 2015
Received in revised form 10 October 2015
Accepted 29 November 2015
Available online 2 December 2015

Keywords:
Accelerometers
Conservative forces
Principal Component Analysis (PCA)
Precise Orbit Determination (POD)
GRACE

ABSTRACT

The accuracy of the conservative force-models is not clear and the new space accelerometers provide a unique opportunity for their validation. In this paper, the conservative-force model deficiencies are investigated via Principal Component Analysis (PCA) using 4 years of GRACE measurements (2006–2009). The deficiencies are assessed by comparing the accelerometer readouts with the differences between the conservative force-model and the precise orbit accelerations. Within this scheme, the spatiotemporal data analysis is synthesized in a time-series of grids whose latitudinal and longitudinal variations are respectively influenced by the half orbital period and the equatorial orbit shift. With maximum amplitude of 50 nm/s^2, the mean map shows a positive overestimation in Canada and Brazil and negative in Greenland. Explaining the 74% of the variability, the two first pairs of PCA modes show un-modeled patterns with amplitudes maxima of 80 nm/s^2 and 50 nm/s^2. Their periodic behavior and wave-length of degree-6 and degree-11s spherical harmonics strongly suggest an additional modeling and improvement. As for the long-term variations, our results show a latitudinal variation of 15 nm/s^2 maximum amplitude correlated with the day-night periods. Performing a combined analysis of ascending and descending orbits, a trend of 3 nm/s^{2}yr in the Indian Ocean is also observed. Our new approach for orbital force-models validation can be considered crucial for the current state-of-the-art of precise orbit determination (POD) and Time–Varying Gravity (TVG) modeling.

1. Introduction

Besides the static mean gravity field (e.g. [14,17,35]), the Time-Varying Gravity (TVG) is a major interest within the fields of satellite gravimetry or mass redistributions in the Earth's system. During the last decade, several TVG series have been computed from Gravity Recovery and Climate Experiment (GRACE) [1,4,11,24,27,41] and employed widely [19,26,34,39,46]. However, those snapshots are available only during the GRACE mission (2002 to now) and several investigations are intended to stabilize their availability with alternative approaches (e.g. [8,9,15,22,45]). Among these studies, the TVG forward modeling or so-called "de-aliasing products" (e.g. [15]) provide time-series of conservative forces which are computed from geophysical models (e.g. NCEP, ECMWF, ECCO, GLDAS/Noah). These models include atmosphere, hydrology and wind-forcing changes in ocean mass. However, the availability and latency of these geophysical models is a serious problem and several approximating analytical models are developed for regular variations and trends (e.g. [2]). For most of satellite missions, the accuracy of the force-models used as input in dynamic and reduced-dynamic POD is not comparable to that of satellite gravimetry or satellite altimetry and the use of TVG can be omitted. For the other missions, however, current standards still fail in covering TVG with analytical models that are real-time functional (pre-processing independency).

Therefore, it should analyze and assess the conservative-force anomalies derived from analytical models, accurate orbit solutions and accelerometer measurements. In the last decade, several studies have examined the ocean-tide models errors by differencing hydrodynamic models (e.g. tide gauges and acoustic tomography) or by running Monte Carlo analyses with inverse models (e.g. [23,36]). Other studies have investigated the sensitivity to different force-models, by evaluating absolute values of root-mean-square fits of observations on orbital arcs (e.g., [10,25,30,38,46]). Despite

* Corresponding author at: Key Laboratory of Planetary Science, Shanghai Astronomical Observatory, Chinese Academy of Sciences, Shanghai 200030, China. Tel.: +86 21 34775292; fax: +86 21 64384618.
E-mail addresses: andres@calabia.com (A. Calabia), sgjin@shao.ac.cn (S. Jin).

http://dx.doi.org/10.1016/j.ast.2015.11.034
1270-9638/

the fact that SLR (satellite laser ranging), DORIS (Doppler Orbitography and Radio positioning Integrated by Satellite), PRARE (Precise Range And Range-rate Equipment) and altimeter measurements have proven to be of practical benefit in these previous studies, little attention has been paid to the instantaneous differences to accelerometer measurements. Since space accelerometers can measure the non-gravitational forces acting on a satellite's surface, we present a new approach to evaluate the error committed in force modeling. On the one hand, accurate accelerometers measure the force needed to keep a proof mass exactly at the spacecraft's center of mass, where the gravity is exactly compensated by the centrifugal force (e.g. onboard GRACE and GOCE). On the other hand, modeled time-varying forces of gravitational origin can be subtracted from precise orbit accelerations to obtain instantaneous POD-based non-gravitational accelerations [5]. Thus, the differences between these two non-gravitational accelerations can provide an assessment about the error committed. Similar approach can be performed to analyze non-gravitational force-models (solar radiation pressure, Earth albedo and atmospheric drag). For these models, a detailed comparison between measurements and modeled surface forces can be found in [18]. The thermal accommodation and the diffuse/specular reflection of incoming particles play an important role under the effects of different densities, temperatures and reflectivity of the different satellite surfaces, usually glass solar arrays and customized functionally graded materials (e.g., [43,44,47]). Since satellite's total accelerations are often not part of the available POD products, the precise reduced-dynamic POD velocities are interpolated and numerically differentiated [6]. This approach serves as a reference to derive precise accelerations from any accurate source, as for example, kinematic GPS, SLR, DORIS or PRARE solutions. Note that the use of instantaneous non-gravitational accelerations instead of orbital arcs, allows analyzing the differences to accurate accelerometer measurements, and yields considerable advantages for many branches of research (e.g. acceleration approach for gravity field recovery, accelerometer calibration, solar radiation pressure, atmospheric drag, tide analysis and TVG validation). In this study, after subtracting the conservative force-model from GOCE's reduced-dynamic POD-based accelerations, the derived solution yielded insufficient accuracy to recover the precise POD-based non-gravitational accelerations. Fortunately, GRACE's orbit solution has proven to provide better results [6], but with several removable periodic errors. Following to this, a purely sinusoidal disturbing signal can be successfully subtracted from the radial axes with smoothing procedures.

In the spatiotemporal data analysis of satellite measurements, the orbital precession represents a major limitation. For that reason, different methods have been employed to avoid this problem (e.g., [13,16,29]). In this paper, the non-gravitational accelerations from GRACE's reduced-dynamic POD are compared to accelerometer measurements and their differences are analyzed in space and time via Principal Component Analysis (PCA). Instead of attempting to estimate principal components with a sequential nonlinear regression analysis of one-dimensional measurements along satellite tracks [28,29], our analysis will examine in detail the covariance matrix of a grid time series, via conventional PCA. Advantages with respect to that technique are discussed in Section 4.

The structure of this article is as follows: Available measurements of GRACE and GOCE are presented in Section 2. Then, POD-based non-gravitational accelerations are briefly introduced with a description of our first results. Moreover, a pilot study performed to derive a complete time series of grids is presented. In Section 3, the PCA is conducted with our computed grids. The results are analyzed and discussed in Section 4. Finally, the summary is given with some recommendations for further study.

2. Observation data

Gravity Recovery and Climate Experiment (GRACE) is a joint mission between the *National Aeronautics and Space Administration* (NASA) in the United States and the *Deutsches Zentrum Für Luft und Raumfahrt* (DLR) in Germany, which has been widely employed in geodesy and climate change applications (e.g. [21] and [20]). GRACE's Level 1B format record files can be downloaded from the Information System and Data Center (ISDC) *GeoForschungsZentrum* (GFZ) website in binary big-endian byte-ordering format [7]. Gravity Field and Steady-State Ocean Circulation Explorer (GOCE) is the first dedicated gravity field mission of the Living Planet Program of the European Space Agency (ESA), and their Level 1B format record files are downloaded from the ESA GOCE Virtual Archive, in text format [40].

The twin satellites of the GRACE mission are equipped with three-axis capacitive Super-STAR accelerometers to measure the non-gravitational forces acting on the satellites. The precision of the X_{SBS} and Z_{SBS} axes is specified to be 0.1 nm/s^2 and 1 nm/s^2 for the Y_{SBS} axes (Satellite Body System). These measurements at a second interval are included in the ACC_1B files. The GOCE mission carry as primary science instrument a gradiometer, consisting of three pairs of accelerometers on orthogonal axes. For two out of three axes, the precision is specified to be 10^{-3} nm/s^2 and an order of magnitude lower for the 3rd axis. The so-called GOCE's common-mode (CM) accelerations provide a very good observation of non-gravitational forces acting on the satellite. Their calibrated measurements at a second interval are included in the EGG_NOM_1b files. The star camera mounted on GRACE satellites provides the precise attitude references to determine the satellite's absolute orientation with respect to the International Celestial Reference System (ICRS). These measurements are given at a 5 s time-sampling interval as a set of quaternion in the SCA_1B GRACE's files. For the GOCE mission, the gradiometer inertial attitude quaternion at a second interval is included in the EGG_NOM_1b files. GRACE's precise position and velocity, at 5 s interval and including formal error, have been computed in a reduced-dynamic POD by the GPS Inferred Positioning System (GIPSY) software of JPL. These solutions are included in the GNV_1B files. Official GOCE's precise position and velocity have been computed in a reduced-dynamic POD by the BERNESE software at the Astronomical Institute of the University of Bern (AIUB). These solutions are included in the SST_PSO_2 files.

3. Methodology

3.1. POD-based non-gravitational accelerations

Since satellite accelerations are not usually provided in the POD solution, these are derived from the precise velocities by means of interpolation and subsequent numerical differentiation [6]. The conservative force-model is the recommended as for Low Earth Orbit (LEO) satellites from the Earth Rotation and Reference Systems Service (IERS) conventions 2010 [32], but with the use of the new ETO11a oceanic tide model. Their components include the EGM2008 [32], the secular variations of its $\bar{C}_{20}$, $\bar{C}_{21}$, $\bar{S}_{21}$, $\bar{C}_{30}$ and $\bar{C}_{40}$ coefficients [32], the Moon and Sun third body tide [31], the solid Earth tides [32], the ocean tides [37], the solid Earth pole tide [32], the ocean pole tide [12] and the relativistic terms [32]. Maximum amplitudes and mean values of all force models on 14 July 2007 are shown in Table 1.

Time-varying Stokes' coefficients up to a degree and order of 120 were computed (including sub-daily variations) under an increment of time sufficiently small to desensitize from discontinuities (∼3600 s). Then, the modeled conservative-force was calculated for every satellite position using the first derivative of the

Table 1
Force models with maximum amplitudes and mean values. Values for GRACE on July 14th, 2007.

Models	Details	Mean (m/s^2)	Max. amplitude (m/s^2)
Earth gravity	EGM2008 with low degree rates. Degree 120.	8.5	6e–2
Third bodies	Moon and Sun from JPL DE421.	1.3e–6	1e–6
Earth tides	Due to Moon and Sun, Wahr terms.	1e–7	8e–7
Ocean tides	EOT11a (256 tides). Degree 120.	0	6e–7
Solid Earth pole tide	IERS 2010 using sub-daily wobble variables	0	2e–8
Ocean pole tide	Desai [12] using sub-daily wobble variables. Degree 120.	0	4e–9
Relativity	Schwarzschild correction.	1.65e–8	2e–10

Table 2
Perturbing signal in POD.

Source	Details	Max. amplitude (m/s^2)
GRACE POD	Systematic error in Z body-frame axes	5e–8
GRACE POD	Systematic error in Y body-frame axes	6e–6
GOCE POD	Systematic error in each of the body-frame axis	1.5e–6

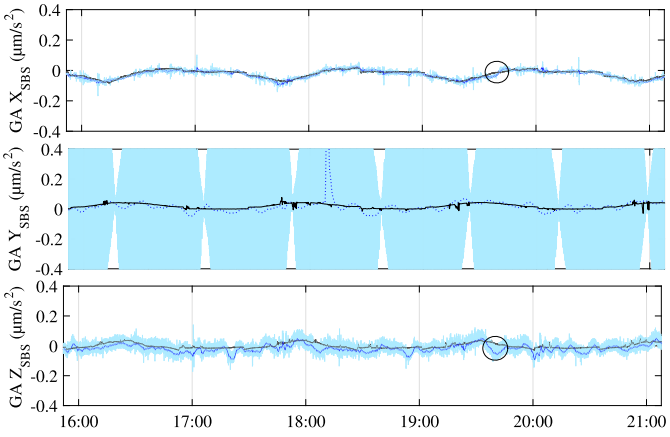

Fig. 1. Accelerations of GRACE-A on July 15th, 2006. The POD-based non-gravitational accelerations are shown in cyan line and the accelerometer measurements in black line. Dotted blue line represents the POD-based non-gravitational accelerations corrected from systematic errors. An un-modeled acceleration is highlighted in a circle. (For interpretation of the references to color in this figure legend, the reader is referred to the web version of this article.)

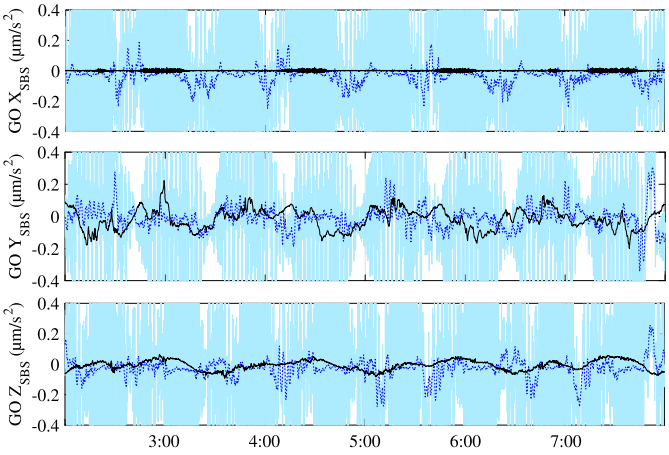

Fig. 2. Accelerations of GOCE on February 15th, 2011. The POD-based non-gravitational accelerations are shown in cyan line and the accelerometer measurements in black line. Dotted blue line represents the smoothed POD-based non-gravitational accelerations. (For interpretation of the references to color in this figure legend, the reader is referred to the web version of this article.)

gravitational potential in Cartesian coordinates [18]. The transformations between reference-systems were performed including sub-daily variations. Diurnal and semi-diurnal ocean tides and nutation contributions were computed and added to the interpolated Earth Orientation Parameters (EOP). After subtracting the conservative force-model from GRACE's reduced-dynamic POD-based accelerations, the systematic error in Z_{SBS} axes [6] was successfully removed by using smoothing techniques. Fig. 1 shows GRACE's POD-based non-gravitational accelerations with respect to the calibrated accelerometer measurements.

Although GRACE's POD perturbing signal was bigger in magnitude, the results from GOCE were worse. After subtracting the conservative force-model from GOCE's POD-based accelerations, a 1.5-hour periodic error of 1.5 μm/s^2 amplitude maxima was detected in all three axes. Fig. 2 shows the GOCE's POD-based non-gravitational accelerations with respect to the calibrated accelerometer measurements. Unfortunately, little improvements were allocated by modeling or smoothing the perturbing signals, and no viable solution could recover the underlying information of GOCE's POD-based non-gravitational forces. Maximum amplitudes of the perturbing signal are shown in Table 2.

3.2. Differences to accelerometer measurements

Due to the difficulty in retrieving GOCE's POD-based non-gravitational accelerations, the PCA analysis was only performed for the GRACE mission. First, 4-year (2006–2009) of measurements were downloaded from the ISDC ftp and processed under MATLAB environment. Then, the differences between computed and measured non-gravitational accelerations were studied along the satellite orbit. Highlighted with a circle in Fig. 1, an overestimation of 1 μm/s^2 in the Z_{SBS} axis shows an un-modeled acceleration at 19:45 h. In the X_{SBS} axis, the highlighted anomaly first overestimates to later underestimate the measured acceleration. Note that the overestimation in the Z_{SBS} axis reaches its maximum when the satellite is over the anomaly. At that position, the difference to the X_{SBS} axis is zero. In order to derive a complete grid of differences, ascending and descending orbits were separated in function of decreasing or increasing spacecraft's latitude. For the development in longitude, the values must be biased 360° after a grid is completed. Therefore, the interpolation and clipping of each grid can be conducted. Different algorithms were compared and the linear interpolation showed the bests results. Interpolated differences between the conservative force-model and the accelerometer measurements in the Z_{SBS} axis are shown in Fig. 3. In this figure, GRACE's descending orbits from 16th to 19th of January 2006 are plotted in dotted line. The time variation is defined from right to left as the equatorial orbit shift precesses westwards, and from North to South as only descending orbits are represented. Note that several anomalies are correlated between continuous orbits.

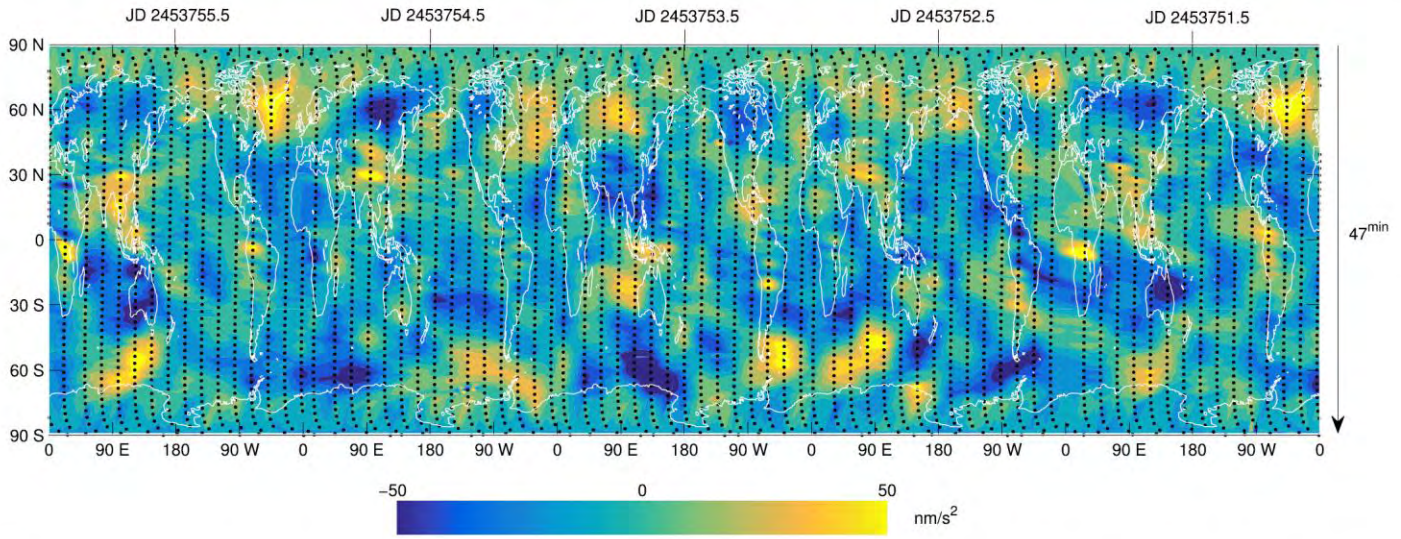

Fig. 3. Interpolation of the differences between the POD-based non-gravitational accelerations and the accelerometer measurements in the Z_{SBS} axis of GRACE's descending orbits. 16th (right) to 19th January (left), 2006, in Julian Date (JD). Dotted line represents the satellite trajectory at 50 s interval.

3.3. Principal component analysis

The spatial patterns of variability, their time variation and the measure of their importance are conducted via the PCA. The aim of this technique is to determine a new set of variables that capture most of the observed variance from the data through a linear combination of the original variables based on Eigen Decomposition. Detailed analyses and the selection of retained modes for static grids can be found in MainPreisendorfer [33] and Wilks [42], and a readily computable algorithm in Bjornsson et al. [3]. Usually, the analysis is presented as dimensionless maps that are often normalized so that the highest value is ± 1. To be adjusted, each spatial pattern is multiplied by the standard deviation of the corresponding temporal component. Therefore, each spatial pattern is considered as an anomaly map with the same units as the original data, and each mode of variability is reconstructed by multiplying the spatial patterns with their corresponding temporal components (time-expansion PCA coefficients). Thus, by summing over only the main set of eigenvectors, noise can be greatly reduced and only physically significant signal remains in the compressed data set.

Since the differences between accelerometer and the POD solution are mainly reflected in the radial direction, only the Z_{SBS} axis is analyzed. For an optimal PCA, the mean value (Fig. 4) has previously been removed from the initial data. The following, is the storage of interpolated differences in a matrix as 1460 grids of 120×60 cells, to subsequently arrange each grid into a row vector, so that the size of the three-dimensional matrix becomes into 7200×1460 cells. Thus, each column can be interpreted as a time series for a given location. After forming the covariance matrix, the eigenvalue problem is easily solved Bjornsson et al., [3]. The solution is a diagonal matrix containing the eigenvalues of the covariance matrix and a matrix of corresponding eigenvectors to each eigenvalue. Each of these eigenvectors can be regarded as a map, and its contribution to the total variability is given by its corresponding eigenvalue. To see how each eigenvector evolves in time, the time-expansion PCA coefficients are calculated as the projections of the initial matrix on each eigenvector.

In this work, the period and the equatorial shift of the orbit both respectively produce a latitudinal and a longitudinal variation, through which each grid is influenced. For the GRACE mission, the orbital period corresponds to 94.10 min and the equatorial orbit shift to 23.6°. Thus, grids and PCA components both vary 3.99 min per westward degree, and 31.37 s per latitudinal degree. The latitudinal component is northwards or southwards depending on using ascending or descending orbits, and cannot be employed together as PCA input, due their different temporal behavior. However, when comparing the PCA results from ascending and descending orbits, these can provide information about short-time variations (not showed in this paper). This last feature will be conducted in future research.

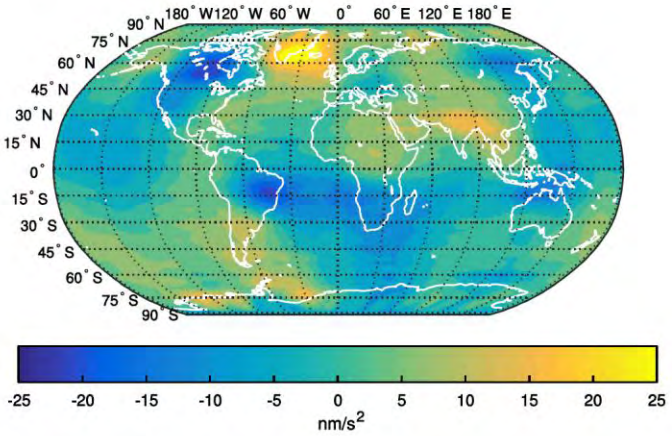

Fig. 4. Mean value of the differences (2006 to 2009) between the POD-based non-gravitational accelerations and the accelerometer measurements of GRACE for the Z_{SBS} axis.

Table 3
Statistical results.

Component	% variance explained	Max. amplitude (m/s^2)
Mean	–	5e−8
PCA1	31%	8e−8
PCA2	22%	8e−8
PCA3	11%	5e−8
PCA4	9%	5e−8
PCA5	5%	1.5e−8

4. Results and discussion

In this paper, 4-year time series of GRACE measurements have been interpolated and converted into grids to investigate the deficiencies in the conservative force-model. The resulting mean-value map (Fig. 4) shows amplitudes maxima of 50 nm/s^2, indicating

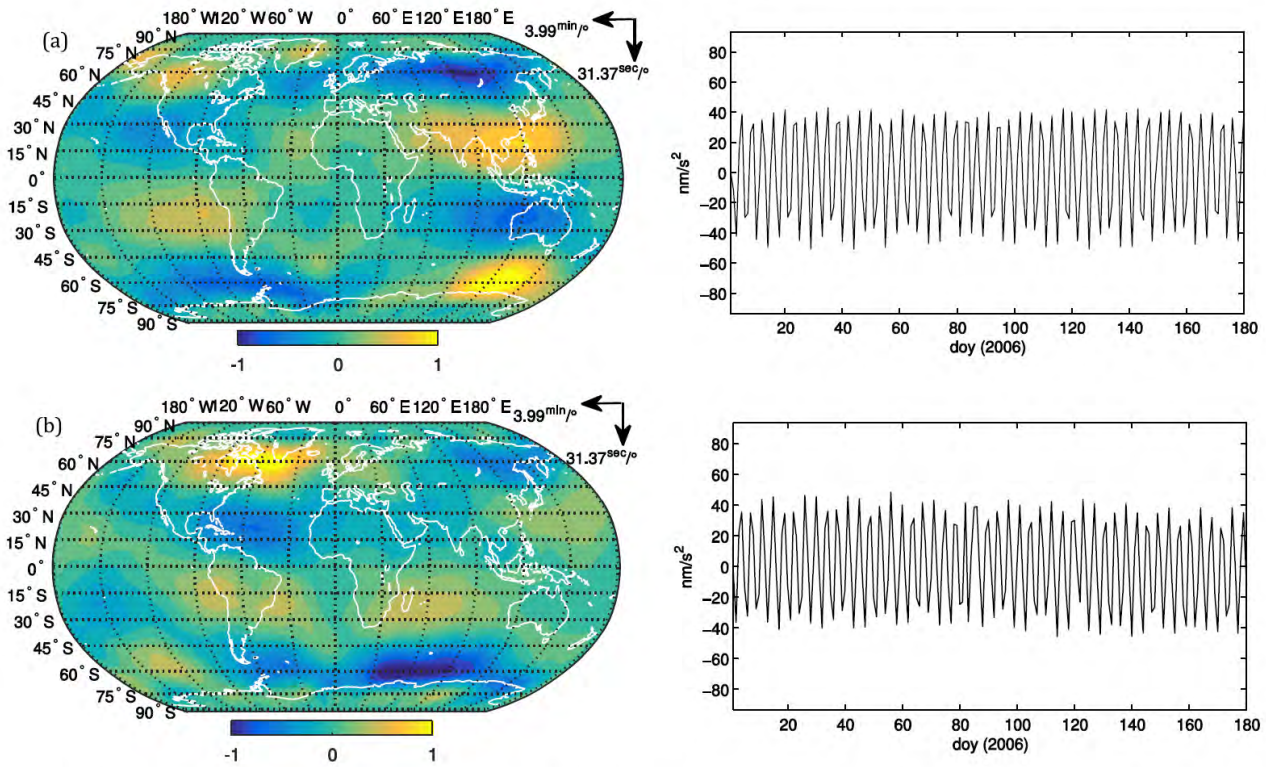

Fig. 5. First (top) and second (bottom) PCA components for the variability of the differences between the POD-based non-gravitational accelerations and the accelerometer measurements (GRACE Z_{SBS} axis, descending orbits, 2006 to 2009). Respectively, 31% and 22% of the variability explained. Maps are time-variable in latitude (31.37 s per southward degree) and longitude (3.99 min per westward degree). Time-expansion PCA coefficients only shown for half year of 2006.

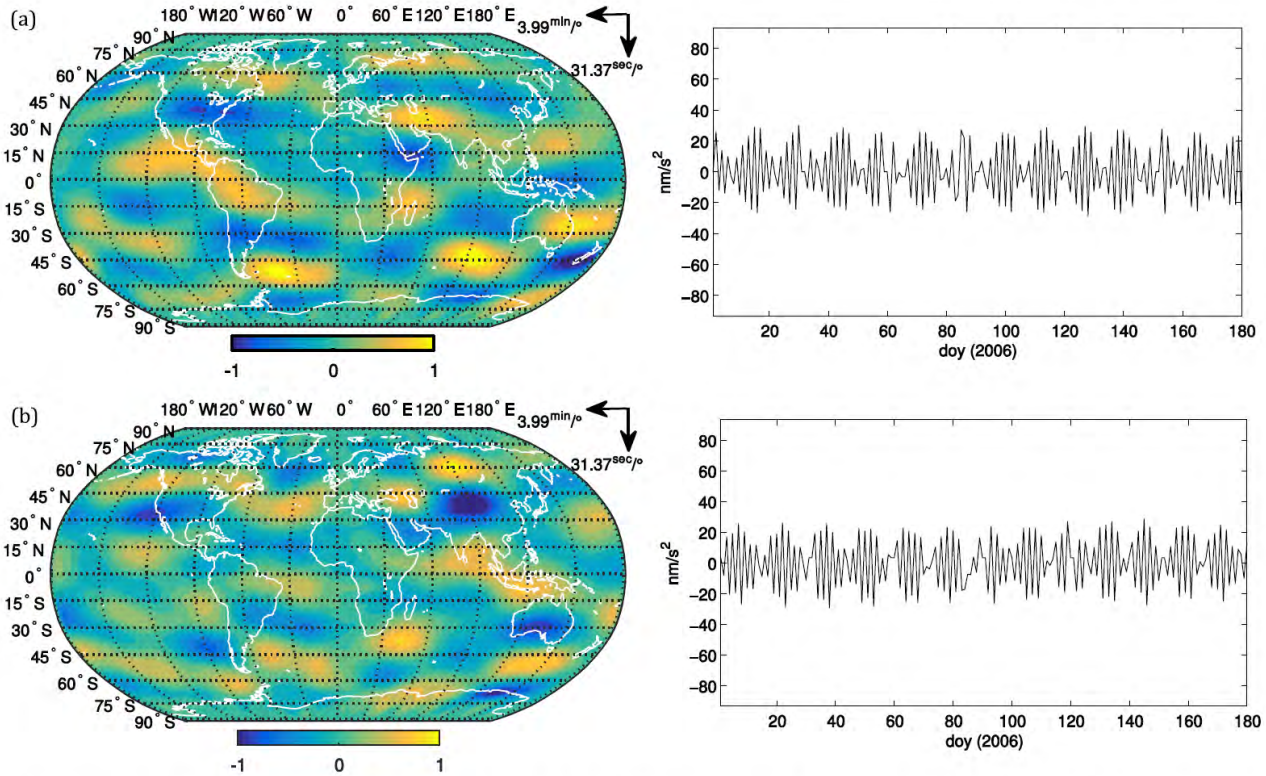

Fig. 6. Third (top) and fourth (bottom) PCA components for the variability of the differences between the POD-based non-gravitational accelerations and the accelerometer measurements (GRACE Z_{SBS} axis, descending orbits, 2006 to 2009). Respectively, 11% and 9% of the variability explained. Maps are time-variable in latitude (31.37 s per southward degree) and longitude (3.99 min per westward degree). Time-expansion PCA coefficients only shown for half year of 2006.

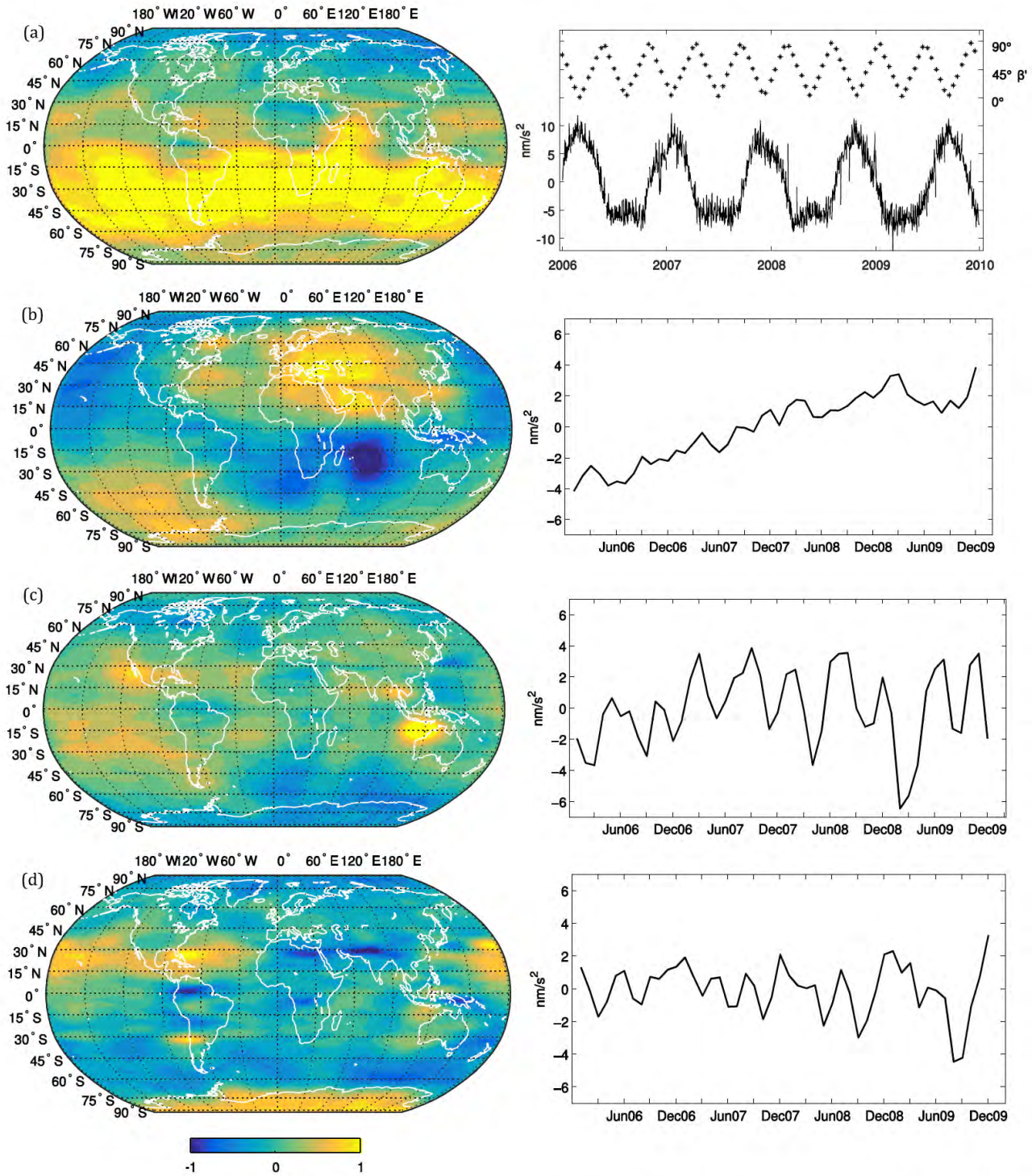

Fig. 7. Long-term variations of the differences between the POD-based non-gravitational accelerations and the accelerometer measurements (GRACE Z_{SBS} axis, 2006 to 2009, descending orbits for (a) and combined solution for (b), (c) and (d)). Right panel in (a) includes the evolution of β' angle values.

a force overestimation at the regions of Canada and Brazil and underestimation in Greenland. In order to determine the spatial patterns of variability, their time variation and the measure of their importance, the analysis has been conducted via the conventional PCA. Maximum amplitudes and percentage of the explained variances are shown in Table 3. With the finality of separating space-time variability, [28] treated the data variability over the course of orbital time (∼90 min for GRACE) to be stationary. In our approach, this variability is regarded as non-stationary, and the analysis can provide information about the variations in the latitudinal dimension. As for the PCA modes, the authors mapped the data to a time-invariant orthogonal basis at every orbit time. In their work, that orthogonal basis is composed by 7 orders of spherical harmonics. Therefore, we might induce that the resolution of their PCA modes must be restricted by the maximum order of the orthogonal basis. In our approach, the resolution of each PCA mode is by nature the pixel size. For instance, our results have provided a pair of PCA modes whose wave-length's order is about the spherical harmonics' degree-11 (Fig. 6). Although these advantages provide several profitable features, the technique used in [28]

seems to provide useful outputs. Nevertheless, we present a more feasible methodology to analyze the sparse satellite measurements along a precessing orbit. Since each derived grid is equally affected in longitude and latitude, the resulting PCA components will follow the same pattern. The resulting two first pair of PCA components shows amplitudes maxima of 80 nm/s^2 and 50 nm/s^2 with a respective wave-length of degree-6 and degree-11s spherical harmonics (Figs. 5 and 6). The four leading eigenvectors together account for 74% of the total variance and, individually, explain 31%, 22%, 11% and 9% of the variance. Unfortunately, their corresponding time-expansion PCA coefficients allocate too low resolution to define periodicities but their spectrum frequency showed strong correlation with eclipse times (not shown in this paper). This correlation might induce that these PCA components represent the reduction of air mass produced by the expansion of atmospheric layers under solar heating. As for long term-variations, the fifth PCA component (Fig. 7(a)) reveals a latitudinal variation defined by 15 nm/s^2 amplitude maxima. This mode is especially correlated to the eclipse times. Note that the amplitude follows the orbital β' angle variation (angle between the Earth–Sun line and the orbit plane). The evolution of β' angle values can be seen at the right panel of Fig. 7(a), where 0° corresponds to alternative midnight and noon times. In this panel, it is clearly seen that descending orbits on February, 2006, e.g., the satellite at noon is affected by a positive force of 10 nm/s^2 in the Southern hemisphere and negative in the Northern hemisphere. On the contrary, at midnight (e.g. on June, 2006), the satellite is affected by a negative force of 5 nm/s^2 in the Southern hemisphere and positive in the Northern hemisphere. As for ascending orbits (not shown in this paper), the results are similar. The next panels (Fig. 7(b)) show a trend of 3 nm/s^2 yr in the Indian Ocean, which might be related to internal geophysical processes. The remaining components (Figs. 7(c) and 7(d)) could be attributed to geodynamical and hydrological processes, as for example, tectonic processes of California, Japan and Indonesia. We should note that the (b), (c) and (d) PCA components from Fig. 7 have been obtained from the monthly mean-averages of combining ascending and descending orbits. The initial idea for this combination was to cancel the binary behavior of the first 4 modes. Another suggestion was to analyze the variations of the time-expansion PCA coefficients with a bigger sampling interval, so multiples of the original frequency can be recovered. The idea of employing ascending and descending orbits to analyze the variations in a shorter time-scale was also considered, but all these suggestions are left for future research.

5. Summary

For most of the satellite missions, the un-precedent accuracy and real-time capability of current analytical force-models make them to become the favorite choice in POD. However, the implications of omitting the use of TVG forward modeling can be a significant concern. In this study, the anomalies to current conservative-force analytical-models are evaluated and analyzed via conventional PCA. Our first results show that precise non-gravitational forces from the GOCE mission cannot be retrieved from the reduced-dynamic POD products, and those from GRACE must be corrected from the purely sinusoidal disturbing signal. In order to study the measurements on time, the differences between the POD-based non-gravitational accelerations and the accelerometer measurements have been interpolated and converted in single grids of ascending and descending orbits. The mean of the differences shows anomalies at Canada, Brazil and Greenland. The variability of each grid can be synthesized in two temporal dimensions: the latitudinal variation, defined by the half orbital period, and the longitudinal variation, defined by the equatorial orbit shift. Using the conventional PCA analysis, our analysis has examined the spatial patterns of variability, their time variation and the measurement of their importance. Our results reveal a latitudinal variation correlated with the day–night periods, a trend in the Indian Ocean and two strong patterns at sub-daily frequencies, also correlated with the day–night periods. Concerning the sub-daily periodicities, the resulting wave-length of degree-6 and degree-11s spherical harmonics suggests a review in the-state-of-the-art of tide-analysis and, preferably, complemented with this methodology and results. In the future, further improvements in our results could be conducted by adding an accurate atmospheric tide model and, in our methodology, by recovering sub-daily periodicities, with the use of both, ascending and descending orbits, or employing multi-satellite approaches.

Conflict of interest statement

The authors declare that there is no conflict of interest regarding the publication of this paper.

Acknowledgement

This work was supported by the National Keystone Basic Research Program (MOST 973) (Grant No. 2012CB72000), National Natural Science Foundation of China (NSFC) Project (Grant Nos. 11173050 and 11373059) and Shanghai Science and Technology Commission Project (Grant No. 12DZ2273300). Great appreciation is extended to ISDC and ESA for providing the data access.

Appendix A. Supplementary material

Supplementary material related to this article can be found online at http://dx.doi.org/10.1016/j.ast.2015.11.034.

References

[1] S. Bettadpur, in: UTCSR Level-2 Processing Standards Document, University of Texas at Austin, Austin, 2012, pp. 327–742 (for Level-2 ProductRelease 0005), GRACE(CSR-GR-12-xx).
[2] R. Biancale, A. Bode, Mean annual and seasonal atmospheric tide models based on 3-hourly and 6-hourly ECMWF surface pressure data, Scientific Technical report STR06/01, Deutsches GeoForschungsZentrum, Potsdam, Germany, 2006.
[3] H. Bjornsson, S.A. Venegas, A manual for EOF and SVD analyses of climatic data, CCGCR report No. 97-1, MCGill University, Montréal, Québec, 1997, 52 pp.
[4] S.L. Bruinsma, J.M. Lemoine, R. Biancale, et al., CNES/GRGS 10-day gravity field models (release 2) and their evaluation, Adv. Space Res. 45 (2010) 587–601.
[5] A. Calabia, S.G. Jin, GPS-based non-gravitational accelerations and accelerometer calibration, in: S. Jin (Ed.), Satellite Positioning: Methods, Models and Applications, InTech-Publisher, Rijeka, Croatia, 2015, pp. 47–72.
[6] A. Calabia, S.G. Jin, R. Tenzer, A new GPS-based calibration of GRACE accelerometers using the arc-to-chord threshold uncovered sinusoidal disturbing signal, Aerosp. Sci. Technol. 45 (2015) 265–271.
[7] K. Case, G. Kruizinga, S. Wu, GRACE Level 1B Data Product User Handbook, 2002 (JPL Publication D-22027).
[8] L. Cerri, J.M. Lemoine, F. Mercier, N.P. Zelensky, F.G. Lemoine, DORIS-based point mascons for the long term stability of precise orbit solutions, Adv. Space Res. 52 (2013) 466–476.
[9] M. Cheng, J.C. Ries, B.D. Tapley, Variations of the Earth's figure axis from satellite laser ranging and GRACE, J. Geophys. Res. 116 (2011) B01409.
[10] A. Couhert, L. Cerri, J.F. Legeais, M. Ablain, N.P. Zelensky, B.J. Haines, F.G. Lemoine, W.I. Bertiger, S.D. Desai, M. Otten, Towards the 1 mm/yr stability of the radial orbit error at regional scales, Adv. Space Res. 55 (2015) 2–23.
[11] C. Dahle, F. Flechtner, C. Gruber, et al., GFZ GRACE, Level-2 processing standards document for level-2 product release 0005. Scientific Technical report STR12/02—data, revised edition, Potsdam, 2013.
[12] S.D. Desai, Observing the pole tide with satellite altimetry, J. Geophys. Res. 107 (C11) (2002) 3186 [Data online]. Available: http://62.161.69.131/iers/conv2010/convupdt/convupdt_c6.html.
[13] F. Gasperini, J.M. Forbes, E.N. Doornbos, S.L. Bruinsma, Wave coupling between the lower and middle thermosphere as viewed from TIMED and GOCE, J. Geophys. Res. Space Phys. 120 (2015).
[14] H. Goiginger, D. Rieser, T. Mayer-Gürr, et al., The combined satellite-only global gravity field model GOCO02S, Geophys. Res. Abstr. 13 (2011) 571, EGU2011-10.

[15] F. Fletcher, 2007 AOD1B product description document. GRACE project documentation, JPL 327–750, Rev. 1.0. JPL, Pasadena, CA, 17 August 2011.
[16] J.M. Forbes, M. Kilpatrick, D. Fritts, A.H. Manson, R.A. Vincent, Zonal mean and tidal dynamics from space: an empirical examination of aliasing and sampling issues, Ann. Geophys. 15 (1997) 1158–1164.
[17] C. Förste, S. Bruinsma, R. Shako, et al., EIGEN-6: a new combined global gravity field model including GOCE data from the collaboration of GFZ-Potsdam and GRGS-Toulouse, in: Ocean Surface Topography Science Team Meeting, San Diego, USA, 2011.
[18] B. Frommknecht, Integrated Sensor Analysis of the GRACE Mission, DGK, Reihe C, Heft 617, Verlag der Bayerischen Akademie der Wissenschaften, 2008.
[19] S.G. Jin, G.P. Feng, Large-scale variations of global groundwater from satellite gravimetry and hydrological models, 2002–2012, Glob. Planet. Change 106 (2013) 20–30.
[20] S.G. Jin, T. van Dam, S. Wdowinski, Observing and understanding the Earth system variations from space geodesy, J. Geodyn. 72 (2013) 1–10.
[21] S.G. Jin, L.J. Zhang, B.D. Tapley, The understanding of length-of-day variations from satellite gravity and laser ranging measurements, Geophys. J. Int. 184 (2) (2011) 651–660.
[22] S.G. Jin, X.G. Zhang, A Tikhonov regularization method to estimate Earth's oblateness variations from global GPS observations, J. Geodyn. 79 (2014) 23–29.
[23] P. Knudsen, O. Andersen, Correcting GRACE gravity fields for ocean tide effects, Geophys. Res. Lett. 29 (8) (2002) 1–4.
[24] J.M. Lemoine, S. Bruinsma, S. Loyer, et al., Temporal gravity field models inferred from GRACE data, Adv. Space Res. 39 (10) (2007) 1620–1629.
[25] F.G. Lemoine, N.P. Zelensky, D.S. Chinn, D.E. Pavlis, D.D. Rowlands, B.D. Beckley, S.B. Luthcke, P. Willis, M. Ziebart, A. Sibthorpe, J.P. Boy, V. Luceri, Towards development of a consistent orbit series for TOPEX, Jason-1, and Jason-2, Adv. Space Res. 46 (2010) 1513–1540.
[26] F.G. Lemoine, N.P. Zelensky, S. Melachroinos, D.S. Chinn, B.D. Beckley, D.D. Rowlands, S.B. Luthcke, GSFC OSTM, Jason-1 and TOPEX POD update, in: Ocean Surface Topography Science Team Meeting, San Diego, USA, 19–21 October 2011.
[27] S.B. Luthcke, D.D. Rowlands, F.G. Lemoine, et al., Monthly spherical harmonic gravity field solutions determined from GRACE inter-satellite range-rate data alone, Geophys. Res. Lett. 33 (2006) L02402.
[28] T. Matsuo, J.M. Forbes, Principal modes of thermospheric density variability: empirical orthogonal function analysis of CHAMP 2001–2008 data, J. Geophys. Res. 115 (2010) A07309.
[29] T. Matsuo, A.D. Richmond, D.W. Nychka, Modes of high latitude electric field variability derived from DE-2 measurements: empirical orthogonal function (EOF) analysis, Geophys. Res. Lett. 29 (7) (2002) 1107.
[30] S. Melachroinos, F. Lemoine, D. Chinn, N. Zelensky, J. Nicholas, B. Beckley, The effect of seasonal and long-period geopotential variations on the GPS orbits, GPS Solut. 18 (4) (2014) 497–507.
[31] O. Montenbruck, E. Gill, Satellite Orbits: Models, Methods and Applications, Springer, Berlin, 2013.
[32] G. Petit, B. Luzum (Eds.), IERS Conventions, IERS Tech. Note, vol. 36, Verlag des Bundesamts für Kartogr. und Geod, Frankfurt am Main, 2010.
[33] R. MainPreisendorfer, Principal Component Analysis in Meteorology and Oceanography, Elsevier, Amsterdam, 1988.
[34] A. Ollivier, Y. Faugere, N. Picot, M. Ablain, P. Femenias, J. Beneveniste, Envisat ocean altimeter becoming relevant for mean sea level trend studies, Mar. Geod. 35 (2012) 118–136.
[35] N.K. Pavlis, S.A. Holmes, S.C. Kenyon, J.K. Factor, The development and evaluation of the earth gravitational model 2008 (EGM2008), J. Geophys. Res. 117 (2012) B04406.
[36] R.D. Ray, R.J. Eanes, G.D. Egbert, N.K. Pavlis, Error spectrum for the global M_2 ocean tide, Geophys. Res. Lett. 28 (2001) 21–24.
[37] D. Rieser, et al., The ocean tide model EOT11a in spherical harmonics representation [Online]. Available: ftp://ftp.dgfi.badw.de/pub/EOT11a, 2012.
[38] S. Rudenko, D. Dettmering, S. Esselborn, T. Schöne, C. Förste, J.M. Lemoine, M. Ablain, D. Alexandre, K.H. Neumayer, Influence of time variable geopotential models on precise orbits of altimetry satellites, global and regional mean sea level trends, Adv. Space Res. 54 (2014) 92–118.
[39] S. Rudenko, M. Otten, P. Visser, R. Scharoo, T. Schone, S. Esselborn, New improved orbit solutions for the ERS-1 and ERS-2 satellites, Adv. Space Res. 49 (8) (2012) 1229–1244.
[40] SERCO/DATAMAT_Consortium, GOCE L1b Products User Handbook, Technical Note GOCE-GSEG-EOPG-TN-06-0137, 2006.
[41] M. Watkins, D.N. Yuan, JPL Level-2 Processing Standards Document for Level-2 Product Release 05. GRACE Document, 2012, pp. 327–744.
[42] D.S. Wilks, Statistical Methods in the Atmospheric Sciences, Academic Press, San Diego, 1995.
[43] A. Tounsi, M.S.A. Houari, S. Benyoucef, E.A.A. Bedia, A refined trigonometric shear deformation theory for thermoelastic bending of functionally graded sandwich plates, Aerosp. Sci. Technol. 24 (2013) 209–220.
[44] A.S. Yahia, A.A. Hassen, H.M.S. Ahmed, A. Tounsi, Wave propagation in functionally graded plates with porosities using various higher-order shear deformation plate theories, Struct. Eng. Mech. 53 (6) (2015) 1143–1165.
[45] N.P. Zelensky, F.G. Lemoine, B.D. Beckley, et al., Improved modeling of time variable gravity for altimeter satellite POD, Poster presented at OSTST, Venice, Italy, 2012.
[46] N.P. Zelensky, F.G. Lemoine, D.S. Chinn, S. Melachroinos, B.D. Beckley, J.W. Beall, O. Bordyugov, Estimated SLR station position and network frame sensitivity to time-varying gravity, J. Geod. 88 (2014) 517–537.
[47] M. Zidi, A. Tounsi, M.S.A. Houarib, E.A.A. Bedia, O.A. Bég, Bending analysis of FGM plates under hygro–thermo-mechanical loading using a four variable refined plate theory, Aerosp. Sci. Technol. 34 (2014) 24–34.